Research Article

Structural, Electronic, Mechanical, Linear and Nonlinear Optical, and Piezoelectric Properties of CsIO₃ Materials from Ab Initio Study

Soraya Belhadj*[1] [iD], Brahim Lagoun[2] [iD], Mohamed Benabdallah Taouti[1] [iD] and Djamal Benbertal[1]

[1] *Laboratory of Physico-Chemistry of Materials (LPCM), Laghouat University, 03000 Laghouat, Algeria*
[2] *Laboratory of Physics of Materials (LPM), Laghouat University, 03000 Laghouat, Algeria*
*Corresponding author: s.belhadj@lagh-univ.dz

Abstract. In order to explore structure-properties relationship, structural, electronic, elastic, optical (linear and nonlinear), piezoelectric, and electro-optic properties of three cesium iodate $CsIO_3$ polymorphs (monoclinic; M, rhombohedric; R, cubic; C) have been computed, discussed and compared by means of density functional theory DFT using the Tran and Blaha modified Becke-Johnson potential TB-mBJ and the Generalized Gradient Approximation GGA implemented in WIEN2K code. Also, the Pseudo-Potential Plane Waves method PP-PW and Local Density Approximation LDA embedded in ABINIT code were used. Calculated structural parameters are in agreement with experimental values with both methods and we found that GGA grades are the closest. Band gaps of M and R systems are both direct (4.00 and 5.13 eV respectively) which apparently increases with increasing structural symmetry. The centrosymmetric cubic system C has no apparent band gap and adopt a metallic behaviour. Noncentrosymmetric M and R phases show interesting piezoelectric and nonlinear optical properties with several similarities in electronic characteristics principally related to the pseudo-rhombohedric structure of the monoclinic M-$CsIO_3$ system.

Keywords. Cesium iodates; Electronic structure; Mechanical properties; Linear and nonlinear optical properties; Piezoelectricity; DFT

PACS. 31.15.A

1. Introduction

Physical and chemical properties of functional iodate-based systems still attract researchers in their investigations [3, 10, 17, 44, 49, 59]. Most works are dealing with structure-properties relationship [9, 26, 27, 32, 50, 58].

In this study, we are interested with cesium iodate $CsIO_3$ compounds. According to experimental results, they exhibit interesting optical properties [62].

As part of the alkali metal iodates family, cesium-based iodates have been the subject of several works. First reports were performed by Wheeler and Barker regarding their synthesis routes [7, 57]. Also, optical properties, growth techniques and vibrational spectra were discussed [4, 6, 11].

Cesium iodate as all simple alkali metal iodates (except sodium iodate) was first characterized as having a cubic structure [28] until 1985 where a new monoclinic $CsIO_3$ polymorph was elaborated [56]. In 2018, Zhang *et al.* [62] hydrothermally prepared single crystals of the third new rhombohedric $CsIO_3$ polymorph.

In addition, via crystal engineering, other mixed Cs-based iodates have been tailored, such as $Cs_2Ge(IO_3)_6$ [29], $Cs(VO)_2O_2(IO_3)_3$ [47], $Cs_2Sn(IO_3)_6$ [20], $Cs_2MoO_3(IO_3)$ [46], $Cs_2[(UO_2)(CrO_4)(IO_3)_2]$ [45, 48].

Besides, some Cs-based nonlinear optical (NLO) crystals (not iodates) are also known and reported in the literature [13, 15, 18, 25, 35, 39, 51, 63].

The purpose of the present paper is to report and to compare results of *ab initio* investigations (based on the density functional theory DFT) of structural, electronic, mechanical, linear and nonlinear optical, and also of piezoelectric properties for the three polymorphs of $CsIO_3$: monoclinic (M), rhombohedric (R), and cubic (C). Our work contains three additional sections starting with the computational details, then results and discussion, and finally the conclusion.

2. Computational Details

The above-mentioned physical properties of the considered compounds are computed using both WIEN2K [12] and ABINIT [16] calculation codes. With the former, Full Potential (all electron) Linearized Augmented Plane Waves method (FP-LAPW) [43], Generalized Gradient Approximation (GGA) in the Perdew, Burke and Ernzerhof parametrisation (PBE08) [33], and Tran and Blaha modified Becke-Johnson potential (TB-mBJ) for exchange correlation (XC) [42, 53] are adopted to evaluate structural, electronic (band structure, electronic density and density of states), and linear optical properties (dielectric function, absorption coefficient, reflectivity, energy-loss function and refractive index). Values of the Muffin-Tin radii R_{MT} for Cs, I and O atoms are 2, 1.8 and 1.4 Bohr respectively and the valence states are respectively $4d^{10}5s^25p^66s^1$, $4d^{10}5s^25p^5$ and $2s^22p^4$ (treated by scalar relativist alongside full relativist treatment of core states). The $R_{MT}K_{max}$ is set to 7. In the irreducible Brillouin zone (IBZ), we use 150k-points to calculate structural and electronic properties and 288k-points to estimate optical properties.

Furthermore, with the later code, we espouse the following details: Pseudo-Potential Plane Waves method (PP-PW) and Local Density Approximation (LDA) [21] for XC potential (PW-LDA) [34], with the Density Functional Perturbation Theory (DFPT) [8]. Structural, elastic, and nonlinear optical, piezoelectric, and electro-optic properties are then computed. Norm-conserving Trouiller-Martin [54] pseudo-potentials generated with the FHI code (Fritz-Haber-Institute) [14] are used with electron valence of Cs, I and O atoms. Structural, elastic and optical properties are extracted using 512-k points and a cut-off energy (E_{cutoff}) of 50eV.

3. Results and Discussion

3.1 Structural Properties

Calculated and experimental structural parameters of monoclinic (M), rhombohedric (R) and cubic (C) cesium iodate $CsIO_3$ are presented in Table 1.

Table 1. Calculated and experimental lattice parameters of $CsIO_3$ polymorphs

		Lattice parameters				
Monoclinic (M)	Method	a (Å)	b (Å)	c (Å)	β	V (Å^3)
	Exp. [56]	6.613	6.613	4.676	90.8	204.47
	GGA	6.657	6.657	4.707	90.8	208.57
	LDA	6.1243	6.1467	4.3244	90.7	162.78
Rhombohedric (R)	Method	a (Å)		c (Å)		V (Å^3)
	Exp. [62]	6.6051		8.087		305.54
	GGA	6.6836		7.6201		294.79
	LDA	6.0410		7.6800		242.72
Cubic (C)	Method	a (Å)				V (Å^3)
	Exp. [61]	4.6620				101.33
	GGA	4.4601				88.72
	LDA	5.5724				173.03

The obtained results for the cell parameters are close to experimental values with tolerable errors between 0.06% and 7.52% leading to volume errors ranging from 2.00% to 20.56% (except for the C phase where errors are much more important). We also observe that almost in general GGA results are overestimated while LDA grades are underestimated (with some exceptions).

3.2 Electronic Properties

3.2.1 Band Structure

Band structures are one of the relevant electronic characteristics in material's properties studies. Figures 1, 2 and 3 present the obtained results of band structure calculations along high symmetry directions in the Brillouin Zone (BZ) for the three polymorphs M, R and C, respectively.
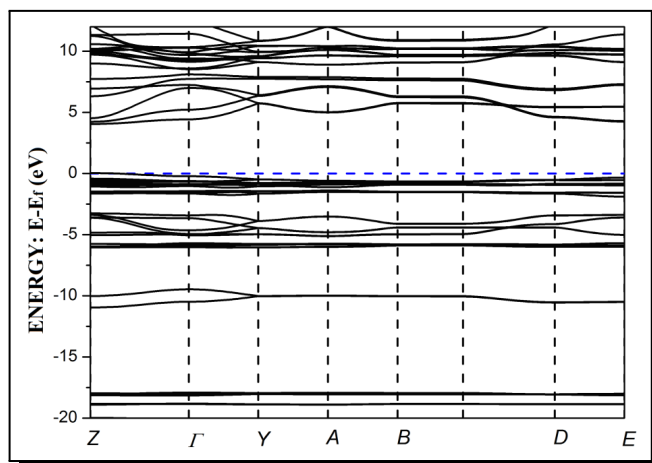
Figure 1. Calculated band structure for monoclinic cesium iodate M-CsIO$_3$
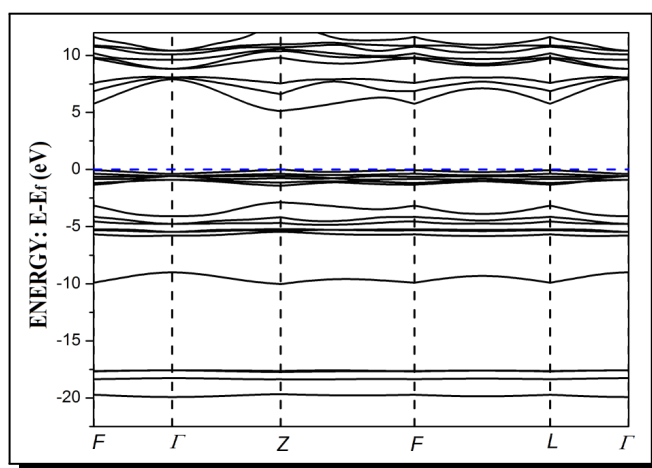
Figure 2. Calculated band structure for rhombohedric cesium iodate R-CsIO$_3$
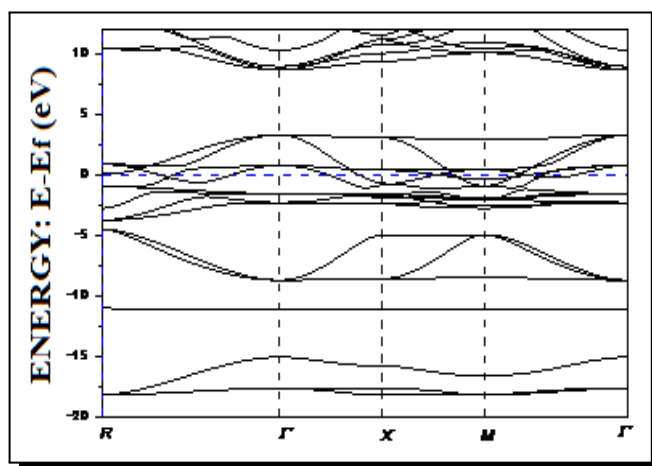
Figure 3. Calculated band structure for cubic cesium iodate C-CsIO$_3$

The obtained results reveal that both M and R phases has direct gap at *Z* point (Figures 1 and 2, respectively) while the C phase displays a metallic characteristic with no apparent

band gap (some bands cross the Fermi level) (Figure 3). Corresponding gap values for M and R systems are 4.00 and 5.13 eV respectively showing up that R compound has higher value of the gap than M compound indicating that both polymorphs possess relatively a high transparency until the mid UV (UV-B) for the former and until the deep UV (DUV or UV-C) for the later. In conclusion, it can be said that the more symmetric is the polymorph the higher is the gap. We mention that obtained band gap values for the two M and R $CsIO_3$ polymorphs are higher than those reported for their monovalent isotypes $RbIO_3$ and $TlIO_3$ (3.82-D and 3.32-I eV) in ref. [9] where the authors also used TB-mBJ method.

3.2.2 Density of State DOS

Since the C phase is centrosymmetric, and from band structure results, it exhibits a metallic characteristic (Figure 3), therefore, in the next sections, we are going to present only results related to M and R phases.

Figures 4 and 5 reflect the calculated total (TDOS) and partial (PDOS) density of states for M and R systems, respectively. Fermi level is set at 0 eV.
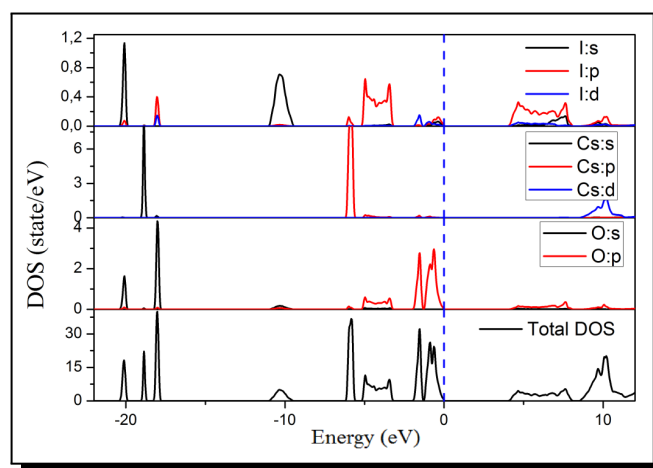
Figure 4. Calculated partial and total DOS for monoclinic M-$CsIO_3$
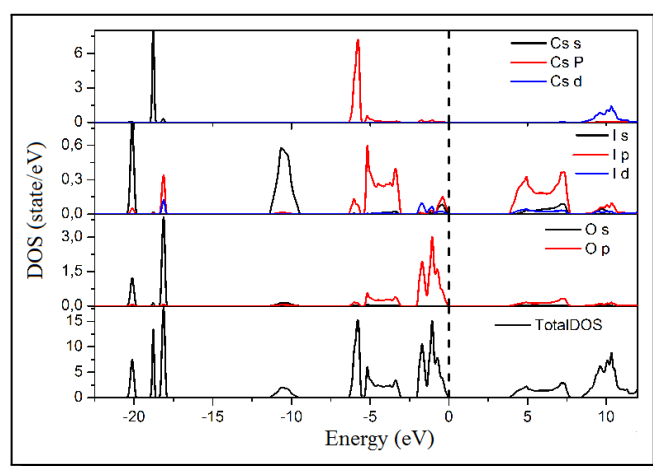
Figure 5. Calculated partial and total DOS for rhombohedric R-$CsIO_3$

From these figures we observe considerable similarities in TDOSs and PDOSs between M-CsIO$_3$ and R-CsIO$_3$ crystals. The states O-s, I-s and Cs-s are present in the bottom of the valence band (VB) while O-p, I-p, and Cs-p states dominate the top of the VB. Moreover, we find out the overlapping of the states O-p and I-p in the VB bottom is an indicator of the probable covalent character of the I-O bond but we observe a sizeable shift between O-p and Cs-p states positions with a narrow overlap indicative of a possible mixed "ionic-less accentuated covalent" Cs-O bond. In the conduction band (CB), there is also some sharing of the Cs-d states.

3.2.3 Charge Density

Planar total charge densities of M and R materials are computed and Figures 6 and 7 illustrate respectively the obtained results in planes containing Cs, I and O atoms.
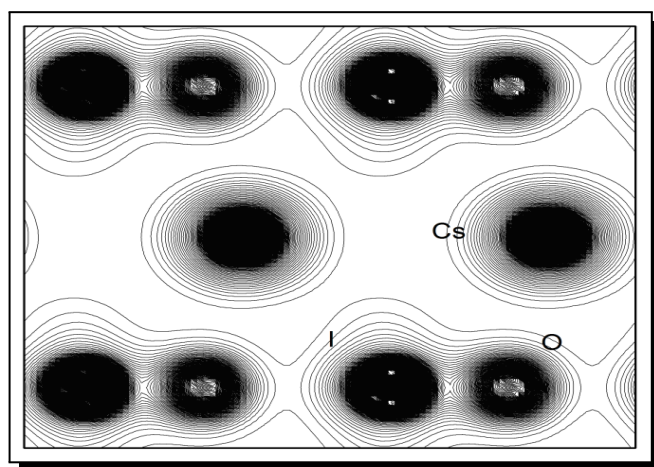
Figure 6. Calculated density of charge for M-CsIO$_3$ in a plane containing Cs, I and O atoms
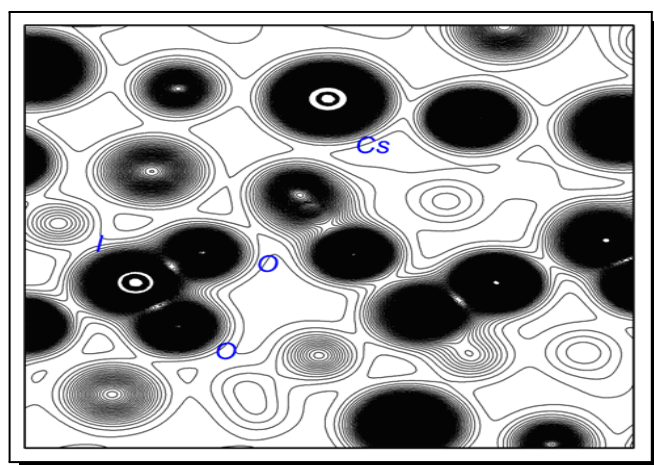
Figure 7. Calculated density of charge for R-CsIO$_3$ in a plane containing Cs, I and O atoms

Obvious similarities are noticed between charge densities of M and R compounds. With both polymorphs, there are clear spherical symmetries of charge densities around Cs atoms with a very slight deviations toward O atoms indicating the predominately ionic Cs-O bond

character. The deformed contours around I and O atoms (with both systems) illustrate the covalent character of I-O bonds. These results are in agreement with DOS outcomes.

In conclusion, the huge resemblance found in electronic properties between M and R phases can be explained by the fact that the M-$CsIO_3$ has a pseudo-rhombohedric structure very close to that of the R-$CsIO_3$ structure.

3.3 Linear Optical Properties

3.3.1 Dielectric Function

The dielectric function $\varepsilon(\omega)$ is a complex, and consists of a real part $\varepsilon_1(\omega)$ and an imaginary part $\varepsilon_2(\omega)$. From the momentum matrix elements between occupied and unoccupied wave functions, the imaginary part of the dielectric function is calculated using equation in ref. [41]. Using Kramers-Kronig transformation, the real part is obtained from the imaginary one [22–24].

Our calculations of the two parts of the dielectric function (as function of photon energy along xx', yy' and/or zz') are plotted in Figures 8 and 9 for M and R phase, respectively.
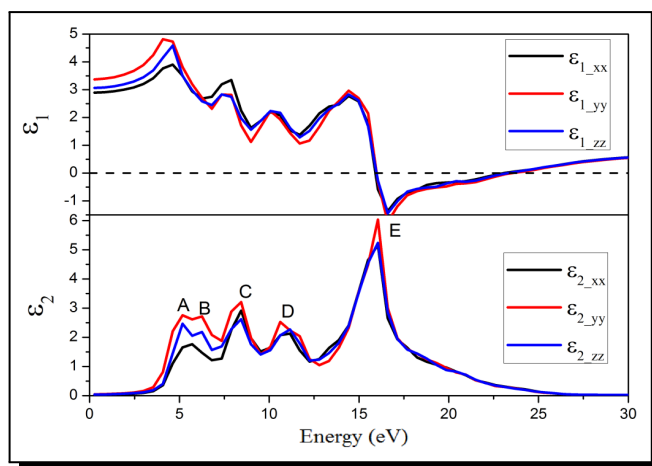
Figure 8. Calculated imaginary and real parts of the dielectric function for M-$CsIO_3$
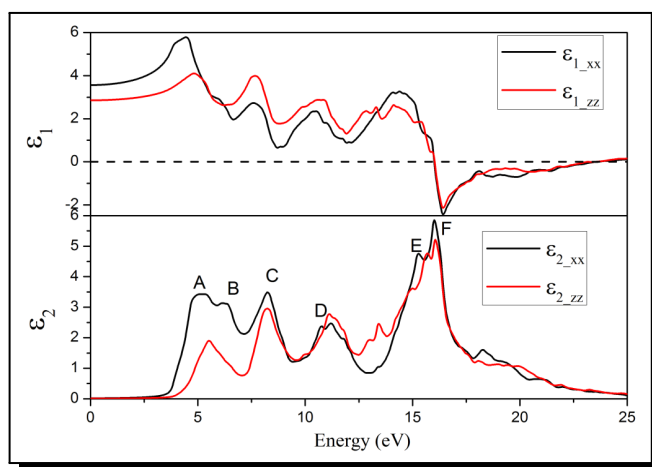
Figure 9. Calculated imaginary and real parts of the dielectric function for R-$CsIO_3$

For the M crystal, there are five main peaks in the imaginary part: A, B, C, D and E (Figure 8). The first two peaks around 5 eV correspond to transitions from O-p (VB) toward I-p (CB). C and D peaks come from transitions of states I-s (VB) and Cs-p (VB) into O-p (CB) and I-p (CB) states. The last peak (E) represents the transitions: I-s (VB) to O-p (CB) and O-s (VB) to I-p (CB).

In the dielectric function plot of R-CsIO$_3$ (Figure 9) six major peaks are distinguished (A, B, C, D, E and F). Those around 5 eV are due to O-2p (VB) to I-5p (CB). Transitions of states I-5p (VB) toward O-2p (CB) states also contribute in that region. In the middle about 10 eV the peaks are mainly due to I-5s (VB) and Cs-5p (VB) into O-2p (CB) and I-5p (CB).

At about 15 eV, we make out transitions of states I-5s (VB) toward O-2p (CB) and of states O-2s (VB) toward I-5p (CB).

3.3.2 Other Linear Optical Properties

Absorption coefficients $I(\omega)$, reflectivity $R(\omega)$, energy-loss function $L(\omega)$ and refractive indices $n(\omega)$ are all deduced from the two parts of the dielectric function [1, 2]. The obtained results are pointed out in Figures 10 and 11 for the M and R phases, respectively.

In the electron energy loss plot $L(\omega)$ (translating the energy loss of a fast electron when traversing the crystal), the firs peak is the plasma frequency peak (where a sharp decrease in reflectivity $R(\omega)$ is noticed) is situated at 24.22 eV and 6.71 eV for M and R systems, respectively.

From absorption spectra $I(\omega)$, we can extract energy values of optical gaps at about 3.54, 2.99 and 3.54 eV (xx', yy' and zz') for M-CsIO$_3$ and 3.85 and 4.45 eV (xx' and zz') for R-CsIO$_3$. These results are in accordance to our band structure grades keeping the same order between the two polymorphs where the R one has in both cases the higher values of gaps. For the R structure, our values are very close but slightly higher (especially in zz' direction) than those experimentally (4.2 eV) and theoretically (3.25 eV) reported in ref. [62] since the authors also used GGA. Therefore, the R compound potentially has wider transparency range and thus may generate higher laser damage threshold (LDT).
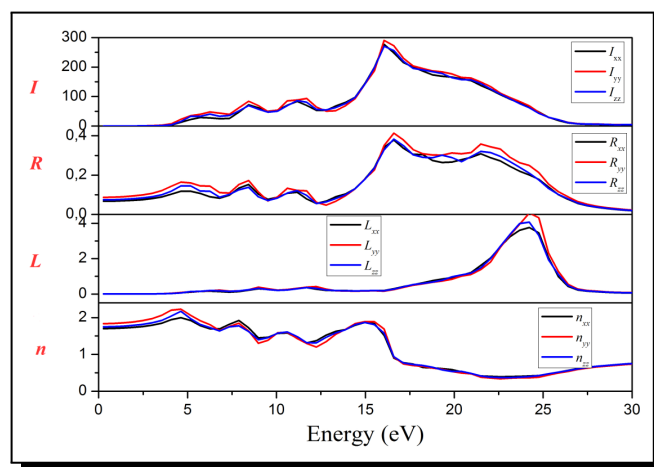
Figure 10. Calculated optical properties for M-CsIO$_3$: absorption coefficient $I(\omega)$ (10^4/cm), reflectivity $R(\omega)$, energy-loss function $L(\omega)$ and refractive indices $n(\omega)$ as function of the incident photon energy
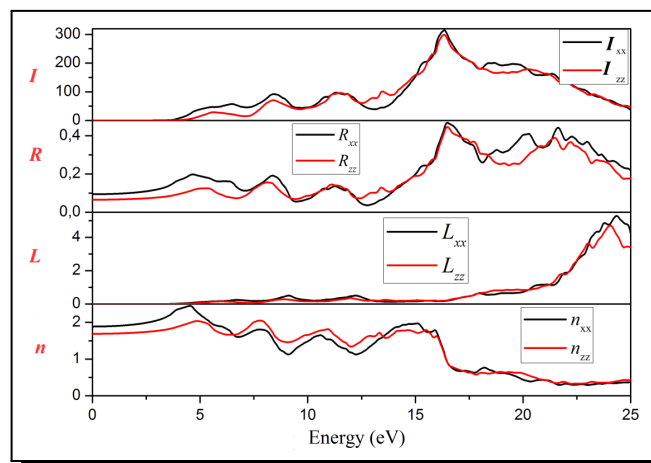
Figure 11. Calculated optical properties for R-CsIO$_3$: absorption coefficient $I(\omega)$ (10^4/cm), reflectivity $R(\omega)$, energy-loss function $L(\omega)$ and refractive indices $n(\omega)$ as function of the incident photon energy

Calculated refractive indices at static limit are 1.70, 1.83, 1.75 (n_{xx}, n_{yy}, n_{zz}) for M-CsIO$_3$ and 1.87, 1.69 (n_{xx}, n_{zz}) for R-CsIO$_3$ (no experimental data is available for comparison) Maximum values are 1.99, 2.23, 2.16 all attained at 4.63 eV, and 2.45, 2.04 (at 4.53, 4.86 eV) for M and R systems respectively, then they decrease gradually to over unity.

3.3.3 Optical Gaps (Birefringence)

The birefringence (difference between each two components of the refractive indices $n(\omega)$) has the following maximum values: 0.26 and 0.16 both at 4.08 eV ($n_{xx'}-n_{yy'}$ and $n_{yy'}-n_{zz'}$) for the M structure and 0.47 at 4.01 eV for the R compound. Corresponding static limit values are 0.14 and 0.09 (M phase), and 0.20 (R phase).
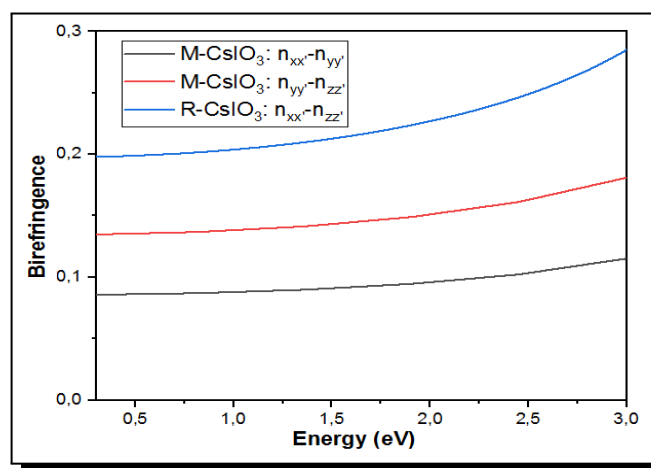
Figure 12. Birefringence of M-CsIO$_3$ and R-CsIO$_3$

At 1064 nm (1.16 eV), birefringence values are 0.088, 0.138, and 0.205 for M ($n_{xx'}-n_{yy'}$, $n_{yy'}-n_{zz'}$) and R phases, respectively (Figure 12). The later value is very close to that found in ref. [13] which is expected since the same approach is used. In all cases, even both polymorphs

are promising birefringents, the R sample has the largest parameters so it is optically more anisotropic.

3.4 Mechanical Properties

In this section, we are going to explore mechanical properties of the three polymorphs (M, R and C) of cesium iodate $CsIO_3$. Since the C phase has no evident electronic properties (metallic character) we include its mechanical properties by means of comparison.

3.4.1 Elastic Coefficients

Cesium iodate $CsIO_3$ in its monoclinic form (crystallising in the m class) has 13 independent elastic constants C_{ij}. The repartition of these coefficients in their respective tensors is as follows [30, 31, 52]:

$$\begin{bmatrix} C_{11} & C_{12} & C_{13} & 0 & C_{15} & 0 \\ & C_{22} & C_{23} & 0 & C_{25} & 0 \\ & & C_{33} & 0 & C_{35} & 0 \\ & & & C_{44} & 0 & C_{46} \\ & & & & C_{55} & 0 \\ & & & & & C_{66} \end{bmatrix}. \tag{1}$$

The stability conditions of the m class are the following [30, 60]:

$$\begin{cases} C_{11}, C_{22}, C_{33}, C_{44}, C_{55}, C_{66} > 0. \\ [C_{11} + C_{22} + C_{33} + 2(C_{12} + C_{13} + C_{23})] > 0. \\ (C_{33}C_{55} - C_{35}^2) > 0. \\ (C_{44}C_{66} - C_{46}^2) > 0. \\ (C_{22} + C_{33} - 2C_{23}) > 0. \\ [C_{22}(C_{33}C_{55} - C_{35}^2) + 2C_{23}C_{25}C_{35} - C_{23}^2 C_{55} - C_{25}^2 C_{33}] > 0. \\ \{2[C_{15}C_{25}(C_{33}C_{12} - C_{13}C_{23}) + C_{15}C_{35}(C_{22}C_{13} - C_{12}C_{23}) \\ \qquad + C_{25}C_{35}(C_{11}C_{23} - C_{12}C_{13})] - [C_{15}^2(C_{22}C_{33} - C_{23}^2) \\ \qquad + C_{25}^2(C_{11}C_{33} - C_{13}^2) + C_{35}^2(C_{11}C_{22} - C_{12}^2)] + C_{55}g\} > 0. \\ \text{with:} \\ g = C_{11}C_{22}C_{33} - C_{11}C_{23}^2 - C_{22}C_{13}^2 - C_{33}C_{12}^2 + 2C_{12}C_{13}C_{23}. \end{cases} \tag{2}$$

The sample R-$CsIO_3$ as a rhombohedric structure (3m crystal class, trigonal system) has six independent elastic constants (C_{11}, C_{12}, C_{13}, C_{14}, C_{33} and C_{44} with $C_{66} = \frac{1}{2}(C_{11} - C_{12})$) distributed as follows [31, 52]:

$$\begin{bmatrix} C_{11} & C_{12} & C_{13} & C_{14} & 0 & 0 \\ & C_{11} & C_{13} & -C_{14} & 0 & 0 \\ & & C_{33} & 0 & 0 & 0 \\ & & & C_{44} & 0 & 0 \\ & & & & C_{44} & C_{14} \\ & & & & & \frac{1}{2}(C_{11} - C_{12}) \end{bmatrix}. \tag{3}$$

The elastic stability criteria for this class are the following [30]:

$$\left\{ \begin{array}{l} C_{11} > |C_{12}| \\ C_{13}^2 < \frac{1}{2}C_{33}(C_{11}+C_{12}) \\ C_{14}^2 < \frac{1}{2}C_{44}(C_{11}-C_{12}) = C_{44}C_{66} \\ C_{44} > 0 \end{array} \right\}. \tag{4}$$

The cubic structure C of cesium iodate crystallizes in the $m\bar{3}m$ class characterized by 03 independent elastic coefficients C_{ij} and their repartition in the tensors is the following [30, 52]:

$$\begin{bmatrix} C_{11} & C_{12} & C_{12} & 0 & 0 & 0 \\ & C_{11} & C_{12} & 0 & 0 & 0 \\ & & C_{11} & 0 & 0 & 0 \\ & & & C_{44} & 0 & 0 \\ & & & & C_{44} & 0 \\ & & & & & C_{44} \end{bmatrix}. \tag{5}$$

The corresponding stability criteria are [30]:

$$\left\{ \begin{array}{l} C_{11}, C_{44} > 0 \\ C_{11} > |C_{22}| \\ C_{11} + 2.C_{12} > 0 \end{array} \right\}. \tag{6}$$

Our obtained results for the three polymorphs are illustrated in Table 2.

Table 2. Elastic coefficients C_{ij} (GPa) calculated for M, R and C polymorohs of $CsIO_3$

	Elastic coefficients C_{ij} (GPa)												
M	C_{11}	C_{12}	C_{13}	C_{15}	C_{22}	C_{23}	C_{25}	C_{33}	C_{35}	C_{44}	C_{46}	C_{55}	C_{66}
	75.8	30.1	33.2	0.32	76.1	50.4	0.09	110.2	−0.14	52.9	−0.03	35	31.4
R	C_{11}	C_{12}		C_{13}		C_{14}		C_{33}		C_{44}		C_{66}	
	114.2	37.2		34.7		−0.00001		97.4		35.7		38.5	
C	C_{11}			C_{12}			C_{44}						
	208.6			−30.1			80.8						

The elastic stability conditions are all satisfied with the three iodates. So, they are mechanically stable.

We observed that coefficients are generally greater with C- then R- then M-$CsIO_3$. In addition, we observe that C_{11}, C_{22} and/or C_{33} are greater than C_{44}, C_{55} and/or C_{66} (for the three systems) reflecting that our considered compounds have better resistance toward contraction than toward shear.

3.4.2 Other Mechanical Parameters

From elastic coefficients, the following parameters can be calculated: Bulk modulus B, Shear modulus G, Young modulus E (in the three notifications; Voigt [55], Reuss [40] and Hill [19]), Poisson ration σ and the B/G ratio (calculated from the three first above mentioned modula).

For the m (M), $3m$ (R) and $m\bar{3}m$ (C) classes, these parameters are determined according to expressions shown in equations (7), (8) and (9), respectively [60].

$$
\left\{
\begin{aligned}
& B_V = \tfrac{1}{9}[C_{11} + C_{22} + C_{33} + 2(C_{12} + C_{13} + C_{23})]. \\
& G_V = \tfrac{1}{15}[C_{11} + C_{22} + C_{33} + 3(C_{44} + C_{55} + C_{66}) - (C_{12} + C_{13} + C_{23})]. \\
& B_R = \Omega[a(C_{11} + C_{22} - 2C_{12}) + b(2C_{12} - 2C_{11} - C_{23}) + c(C_{15} - 2C_{25}) \\
& \qquad + d(2C_{12} + 2C_{23} - C_{13} - 2C_{22}) + 2e(C_{25} - C_{15}) + f]^{-1}. \\
& G_R = 15\{4[a(C_{11} + C_{22} + C_{12}) + b(C_{11} - C_{12} - C_{23}) + c(C_{15} + C_{25}) \\
& \qquad + d(C_{22} - C_{12} - C_{23} - C_{13}) + e(C_{15} - C_{25}) + f]/\Omega \\
& \qquad + 3[g/\Omega + (C_{44} + C_{66})/(C_{44}C_{66} - C_{46}^2)]\}^{-1}. \\
& a = C_{356}C_{55} - C_{35}^2,\, b = C_{23}C_{55} - c_{25}C_{35},\, c = C_{13}C_{35} - C_{15}C_{33} \\
& d = C_{13}C_{55} - C_{15}C_{35},\, e = C_{13}C_{25} - C_{15}C_{23} \\
& f = C_{11}(C_{22}C_{55} - C_{25}^2) - C_{12}(C_{12}C_{55} - C_{15}C_{25}) + C_{15}(C_{12}C_{25} - C_{15}C_{22}) \\
& \qquad + C_{25}(C_{23}C_{35} - C_{25}C_{33}). \\
& g = C_{11}C_{22}C_{33} - C_{11}C_{23}^2 - C_{22}C_{13}^2 - C_{33}C_{12}^2 + 2C_{12}C_{13}C_{23}. \\
& \Omega = 2[C_{15}C_{25}(C_{33}C_{12} - C_{13}C_{23}) + C_{15}C_{35}(C_{22}C_{13} - C_{12}C_{23}) \\
& \qquad + C_{25}C_{35}(C_{11}C_{23} - C_{12}C_{13})] - [C_{15}^2(C_{22}C_{33} - C_{23}^2) \\
& \qquad + C_{25}^2(C_{11}C_{33} - C_{13}^2) + C_{35}^2(C_{11}C_{22} - C_{12}^2)] + gC_{55}.
\end{aligned}
\right\}
\tag{7}
$$

$$
\left\{
\begin{aligned}
& B_v = \tfrac{1}{9}[2(C_{11} + C_{12}) + 4.C_{13} + C_{33}] \\
& B_R = c^2/M; \qquad\qquad\quad c^2 = (C_{11} + C_{12})C_{33} - 2C_{13}^2 \\
& \qquad\qquad\qquad\qquad\quad M = C_{11} + C_{12} + 2C_{33} - 4C_{13} \\
& B_H = \tfrac{1}{2}(B_V + B_R) \\
& G_V = \tfrac{1}{30}[M + 12(C_{44} + C_{66})] \\
& G_R = \tfrac{5}{2}\{c^2.a/[3.B_V.a + c^2(C_{44}.C_{66})]\}; \quad a = C_{44}.C_{66} - C_{14}^2 \\
& G_H = \tfrac{1}{2}(G_V + G_R)
\end{aligned}
\right\}.
\tag{8}
$$

$$
\left\{
\begin{aligned}
& B_V = B_R = (C_{11} + 2C_{12})/3. \\
& G_V = (C_{11} - C_{12} + 3C_{44})/5. \\
& G_R = 5(C_{11} - C_{12})C_{44}/[4C_{44} + 3(C_{11} - C_{12})].
\end{aligned}
\right\}.
\tag{9}
$$

For the three phases, we consider the following formulas to calculate Young's modulus E_i in the three notations, the three moduli in the Hill notation M_H ($M = B$, G ou E), and Poisson's ratio σ [60]:

$$
\left\{
\begin{aligned}
& E_i = 9B_iG_i/(3B_i + G_i) \qquad i = V, R, ouH \\
& M_H = \tfrac{1}{2}(M_R + M_V), \qquad M = B, G, E. \\
& \sigma = (3B_H - 2G_H)/[2(3B_H + GH)]
\end{aligned}
\right\}.
\tag{10}
$$

The obtained values are shown in Table 3.

Table 3. Bulk B, Shear G and Young E moduli, Poisson's ratio σ and the B/G ratio calculated for M-, R- and C-CsIO$_3$ polymorphs

Modulus	B (GPa)			G (GPa)			E (GPa)			Ratio	
Phase	B_V	B_R	B_H	G_V	G_R	G_H	E_V	E_R	E_H	σ	B/G
M	54.41	51.38	52.90	33.74	30.09	31.91	83.88	75.52	79.71	0.2488	1.6575
R	59.88	59.48	59.68	36.60	35.50	36.05	91.22	88.82	90.02	0.2486	1.6555
C	49.88	49.48	49.48	96.21	92.78	94.49	175.13	171.29	173.22	−0.083	0.5237

From Table 3 we detect that all M_i parameters are greater for C-CsIO$_3$ except the B_is (which are most important with R-CsIO$_3$ (Figures 13 and 14). These results can be explained by the fact that B_i grades are related to the cell parameters a and c and therefore directly related to values of the cell volume (Figure 13) and also that G_i and E_i increase with increasing polymorph symmetry (C>R>M). Moreover, σ and B/G ratios adopt the following order: M≥R>C and the nearby zero value of σ for the M compound is an indicator of its metallic behaviour.
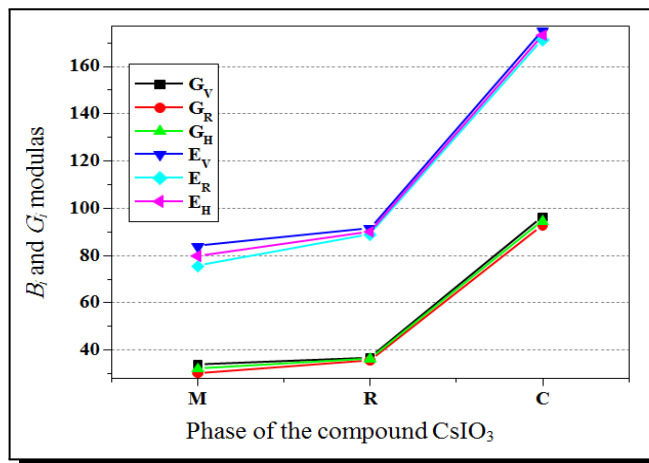
Figure 13. Relation between Bulk G_i and Young E_i moduli for the CsIO$_3$ phases
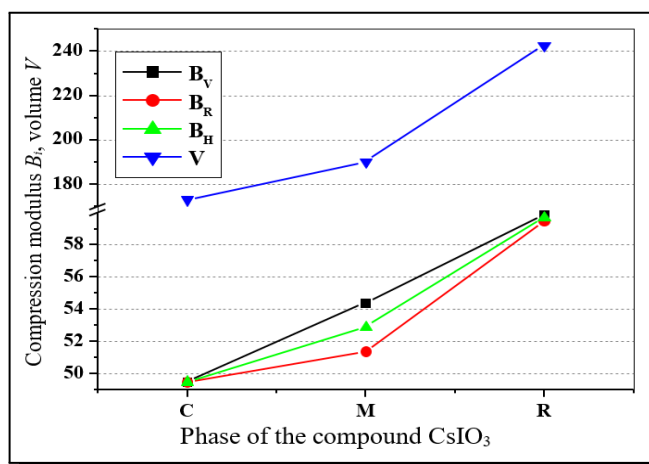
Figure 14. Relation between Shear modulus B_i and volume V for the CsIO$_3$ phases

The ratio B/G is used to determine if a material is brittle or tough (malleable); if $B/G > 1.75$ then the material is tough, whereas if $B/G < 1.75$ that means that it is brittle [37]. According to values in Table 3, our materials are all brittle (difficult to sharp).

The Poisson's ratio σ is also another criterion of brittleness and malleability such as $\sigma > 0.26$ we have a tough crystal and $\sigma < 0.26$ the system is brittle [40] and our results are consistent with these norms confirming B/G results that our three polymorphs are all brittle.

3.4.3 Elastic Anisotropy

We calculated the anisotropy international index A^U according to equation (11) [38] and the found values are reported in Table 4.

$$\left\{ A^U = 5\frac{G_V}{G_R} + \frac{B_V}{B_R} - 6 \geq 0 \right\}. \tag{11}$$

Table 4. Elastic anisotropy A^U of M, R and C phases of $CsIO_3$ compound

Material	M-CsIO$_3$	R-CsIO$_3$	C-CsIO$_3$
A^U	0.66	0.16	0.18

We evidently conclude that our phases are all anisotropic (positive values of A^U) and that M-CsIO$_3$ is the most anisotropic followed by C and R (the two later having close values).

To more illustrate the elastic anisotropic character of the studied structures, we plotted the bulk modulus B and the Young's modulus E in two dimensions (2-D) and three dimensions (3-D). Figures 15-20 demonstrate the obtained plots for M, R and C phases, respectively.

According to Figures 15 and 16, the monoclinic cesium iodate M-CsIO$_3$ clearly shows enhanced elastic anisotropy in the three directions (important deviation from sphericity with both bulk and Young moduli).
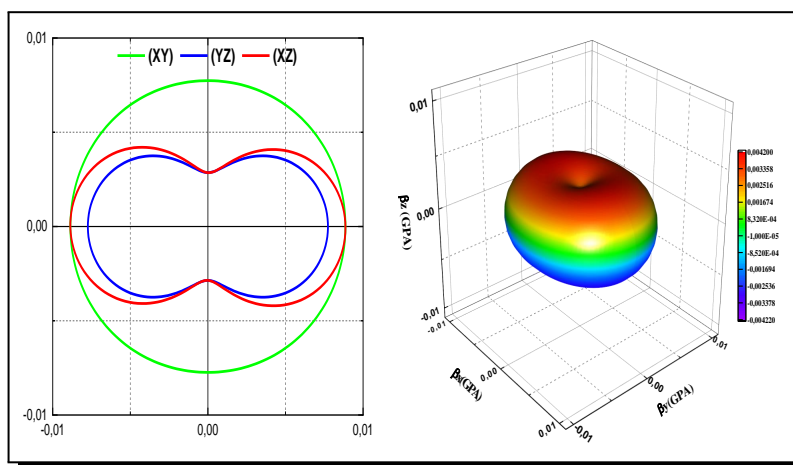
Figure 15. Bulk modulus B of the M-CsIO$_3$ in 2-D (left) and 3-D (right)
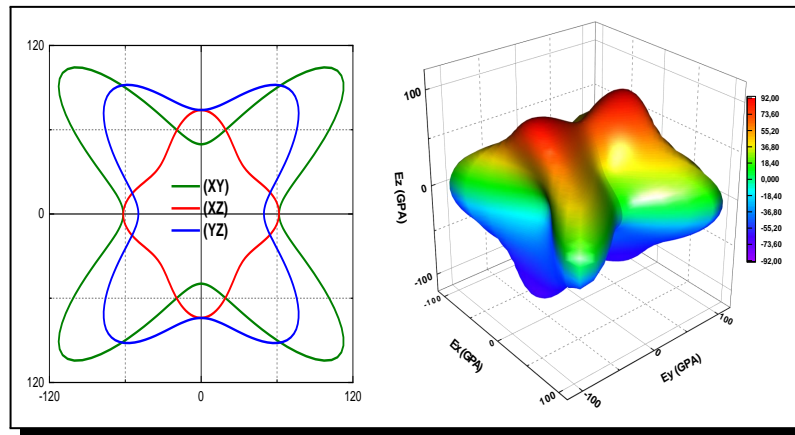
Figure 16. Young modulus E of the M-CsIO$_3$ in 2-D (left) and 3-D (right)

For R structure, there is some deviation from spherical shape with both moduli but less important in (xy) direction (Figures 17 and 18).
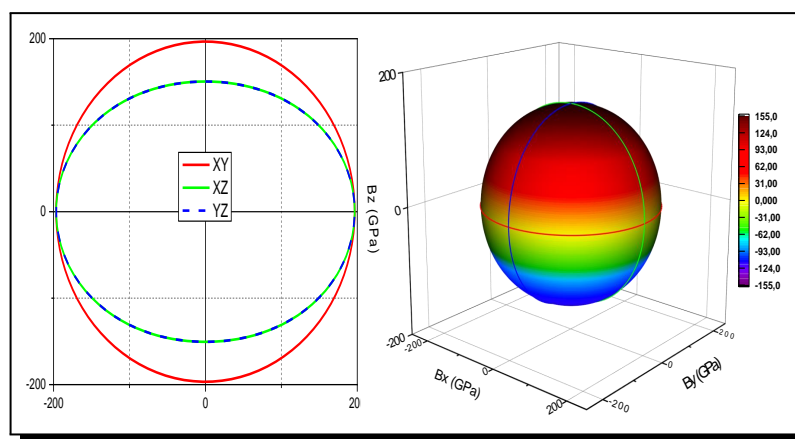
Figure 17. Bulk modulus B of the R-CsIO$_3$ in 2-D (left) and 3-D (right)
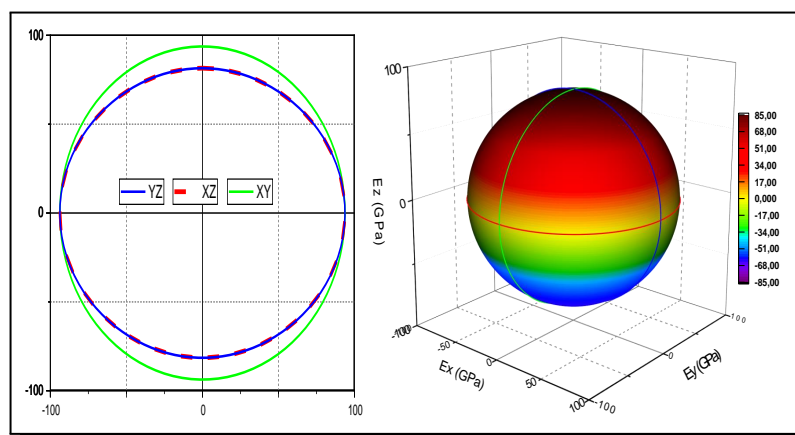
Figure 18. Young's modulus E of the R-CsIO$_3$ in 2-D (left) and 3-D (right)

The cubic phase is obviously isotopic according to bulk plots (Figures 19) but from Figure 20 it is clearly anisotropic and with an identical behaviour in the three directions (xy, xz and yz).
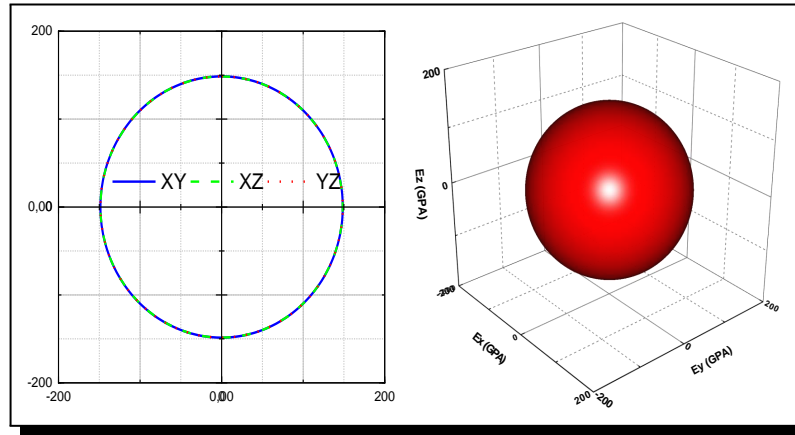
Figure 19. Bulk modulus B of the C-CsIO$_3$ in 2-D (left) and 3-D (right)
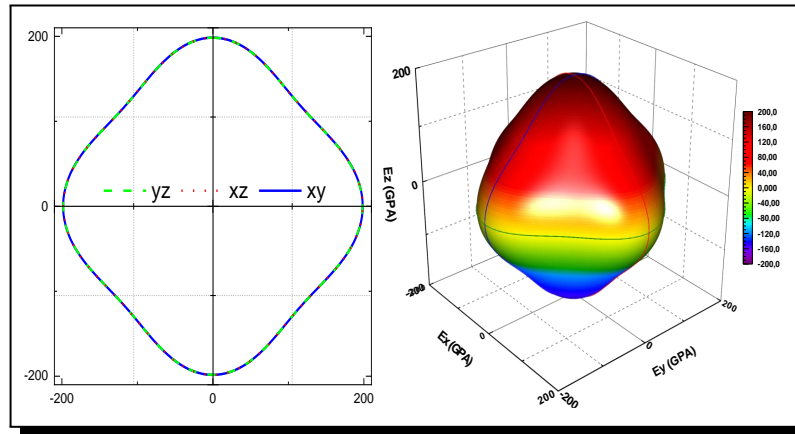
Figure 20. Young modulus E of the C-CsIO$_3$ in 2-D (left) and 3-D (right)

In the next sections, cubic cesium iodate is not considered since it is centrosymmetric and does not own piezoelectric and nonlinear optical (NLO) properties.

3.5 Piezoelectric Properties

As linear optical properties, piezoelectric coefficients of M (11 coefficients) and R (4 coefficients) phases are distributed according to equations 12 and 13 respectively [30, 31, 52] (the C system being centrosymmetric does not possess piezoelectric properties) and the results are reported in Table 5.

$$\begin{bmatrix} d_{11} & d_{12} & d_{13} & 0 & d_{15} & d_{16} \\ 0 & 0 & 0 & d_{24} & 0 & d_{26} \\ d_{31} & d_{32} & d_{33} & 0 & d_{35} & 0 \end{bmatrix}, \tag{12}$$

$$\begin{bmatrix} 0 & 0 & 0 & 0 & d_{15} & -2d_{22} \\ -d_{22} & d_{22} & 0 & d_{15} & 0 & 0 \\ d_{31} & d_{31} & d_{33} & 0 & 0 & 0 \end{bmatrix}. \tag{13}$$

From a general inspection of the results, the monoclinic compound M acquires larger coefficients but d_{31} and d_{33} are greater with R-phase.

Table 5. Piezoelectric coefficients d_{ij} (pc/N) calculated for M-CsIO$_3$ and R-CsIO$_3$

Phase	Piezoelectric coefficient d_{ij} (pc/N)										
M	d_{11}	d_{12}	d_{13}	d_{15}	d_{16}	d_{24}	d_{26}	d_{31}	d_{32}	d_{33}	d_{35}
	15.2	16.9	−12.1	−0.24	9E-5	−0.06	37.74	−0.03	−9E-3	−0.03	1.99
R	d_{15}			d_{22}			d_{31}			d_{33}	
	−32.06			−42E-7			−4.27			−8.16	

The maximum values are $|d_{15}| = 32.06$ (for R) and $d_{26} = 37.74$ (for M) which are close to each other. This is possibly due to the pseudo-rhombohedric structure of the M-phase with $a \approx b \neq c$ and $\beta = 90.8° \approx 90°$. In conclusion, more the material is structurally symmetric less it has important piezoelectricity. Finally, we can say that M-CsIO$_3$ is more piezoelectric.

3.6 Nonlinear Optical (NLO) Properties
NLO properties reported in this section are electrooptic coefficients r_{ij} and second order optical coefficients d_{ij}.

3.6.1 Electrooptic Coefficients
The independent electrooptic coefficients of the m class (M phase) are 10 (r_{11}, r_{13}, r_{21}, r_{23}, r_{31}, r_{33}, r_{42}, r_{51}, r_{53} and r_{62}) and of the 3m class (R phase) are 4 (r_{11}, r_{13}, r_{33} and r_{51}). Their distribution in the corresponding tensors are shown in equations (14) and (15), respectively [5].

$$\begin{bmatrix} r_{11} & 0 & r_{13} \\ r_{21} & 0 & r_{23} \\ r_{31} & 0 & r_{33} \\ 0 & r_{42} & 0 \\ r_{51} & 0 & r_{53} \\ 0 & r_{62} & 0 \end{bmatrix}, \tag{14}$$

$$\begin{bmatrix} r_{11} & 0 & r_{13} \\ -r_{11} & 0 & r_{13} \\ 0 & 0 & r_{33} \\ 0 & r_{51} & 0 \\ r_{51} & 0 & 0 \\ 0 & -r_{11} & 0 \end{bmatrix}. \tag{15}$$

Table 6 illustrate our obtained values of electro-optic coefficients r_{ij} (pc/N) for M and R phases of the CsIO$_3$ compound.

Table 6. Calculated electro-optic coefficients r_{ij} (pc/N) of monoclinic and rhombohedriccesium iodate

Phase	Electrooptic coefficients r_{ij} (pc/N)									
M	r_{11}	r_{13}	r_{21}	r_{23}	r_{31}	r_{33}	r_{42}	r_{51}	r_{53}	r_{62}
	12.93	0.03	10.09	0.03	−0.06	−0.16	−12E-5	−85E-4	0.23	11.23
R	r_{11}		r_{13}		r_{33}			r_{51}		
	−5.56		−8.40		−11.48			−10.14		

Both systems have comparable values of r_{ij}, nevertheless those important with R phase are neglected with M phase (around zero) except for r_{11}.

Maximum values are $r_{11} = 12.93$ for M and $r_{33}| = 11.48$ for R indicating that the former is slightly more electro-optic than the later considering the pseudo-rhombohedric structure of M.

3.6.2 Second Order Optical Coefficients

Ten (10) second order optical coefficients characterized the m class while the 3m class is characterized by only three coefficients (eq. (16) and eq. (17), respectively [36]).

$$\begin{bmatrix} d_{11} & d_{12} & d_{13} & 0 & d_{15} & 0 \\ 0 & 0 & 0 & d_{24} & 0 & d_{26} \\ d_{31} & d_{32} & d_{33} & 0 & d_{35} & 0 \end{bmatrix}, \tag{16}$$

$$\begin{bmatrix} 0 & 0 & 0 & 0 & d_{31} & -d_{22} \\ -d_{22} & d_{22} & 0 & -d_{22} & 0 & 0 \\ d_{31} & d_{31} & d_{33} & 0 & 0 & 0 \end{bmatrix}. \tag{17}$$

In Table 7, second order optical properties of both polymorphs are reported.

Table 7. Second order optical coefficients d_{ij} calculated for M and R polymorphs of $CsIO_3$

Phase	Second order coefficient d_{ij} (pm/V)									
M	d_{11}	d_{12}	d_{13}	d_{15}	d_{24}	d_{26}	d_{31}	d_{32}	d_{33}	d_{35}
	-19.32	-14.17	-3.05	0.031	-0.087	-14.17	0.031	-0.087	-0.31	-3.05
R	d_{22}			d_{31}				d_{33}		
	0.00			14.06				16.83		

M and R phases present maximum grades at $|d_{11}| = 19.32$ (by analogy with r_{11} as maximum value) and $d_{33} = 16.83$ (by analogy with r_{33} as maximum) respectively showing up that the monoclinic polymorph exhibit somewhat a better second order optical character than the rhombohedric polymorph (taking into account the pseudo-rhombohedric structure of the M phase).

4. Conclusion

The aim of the present work is the theoretical investigation of structural, electronic, mechanical and optical properties of three cesium iodate $CsIO_3$ polymorphs; monoclinic (M), rhombohedric (R) and cubic (C) by means of density functional theory (DFT). The calculated structural parameters by the two methods (GGA and LDA) are in good agreement with experimental ones especially those obtained with GGA method (with some exceptions).

Most considered properties are intrinsically related to the difference in structure from one polymorph to another. Monoclinic system M-$CsIO_3$ displays higher birefringence, Poisson ratio σ, B/G ratio and elastic anisotropy, and also better piezoelectric and nonlinear optical properties while its cubic structure (C) has enhanced resistance toward compression and toward shear and elevated values of shear G_i and Young E_i moduli. In the case of R-$CsIO_3$, it has superior band gap value (C phase having metallic characteristic), higher bulk modulus B_i, but in particular,

its piezoelectric and nonlinear optical tendencies are less but close to those found for monoclinic $CsIO_3$ which is explained by the pseudo-rhombohedric structure of the later. In conclusion, M-$CsIO_3$ is a better mechanical, nonlinear, and piezoelectric functional material while R-$CsIO_3$ is a better electro-optic functional material.

Acknowledgments

Competing Interests

The authors declare that they have no competing interests.

Authors' Contributions

All the authors contributed significantly in writing this article. The authors read and approved the final manuscript.

References

[1] R. Abt, C. Ambrosch-Draxl and P. Knoll, Optical response of high temperature superconductors by full potential LAPW band structure calculations, *Physica B: Condensed Matter* **194–196, Part 2** (1994), 1451 – 1452, DOI: 10.1016/0921-4526(94)91225-4.

[2] C. Ambrosch-Draxl and J. O. Sofo, Linear optical properties of solids within the full-potential linearized augmented planewave method, *Computer Physics Communications* **175** (2006), 1 – 14, DOI: 10.1016/j.cpc.2006.03.005.

[3] Y. An, Y. Zhong, T. Sun, H. Wang, Z. Hu, H. Liu, S. Liu, Y. Kong and J. Xu, Synthesis, structure and characterizations of $M(IO_3)_2(HIO_3)$ (M = Ca, Sr), new anhydrous alkaline earth metal bis-iodatehydrogeniodate compounds, *Dalton Transactions* **48** (2019), 13074 – 13080, DOI: 10.1039/C9DT02575H.

[4] A. F. Armington and J. J. O'Connor, Gel growth of iodate crystals, *Materials Research Bulletin* **6**(4) (1971), 653 – 658, DOI: 10.1016/0025-5408(71)90098-5.

[5] A. Authier, *International Tables for Crystallography, Volume D: Physical Properties of Crystals*, Kluwer Academic Publishers (2003).

[6] T. G. Balicheva and G. A. Petrova, Vibrational spectra of the IO_3-ion in alkali iodates, *Journal of Structural Chemistry* **14** (1973), 424 – 430, DOI: 10.1007/BF00746993.

[7] T. V. Barker, II.—Note on the iodates and periodates of the alkali metals and the ammonium radical, Iodates and periodates of the alkali metals, *Journal of the Chemical Society, Transactions* **93** (1908), 15 – 17, DOI: 10.1039/CT9089300015.

[8] S. Baroni, S. de Gironcoli, A. Dal Corso and P. Giannozzi, Phonons and related properties of extended systems from density-functional perturbation theory, *Reviews of Modern Physics* **73** (2001), 515 – 567, DOI: 10.1103/RevModPhys.73.515.

[9] S. Belhadj, B. Lagoun, M. B. Taouti, S. Khenchoul, A. Benghia and D. Benbertal, *TB-mBJ* calculation of structural, electronic and optical properties of two monovalent iodates AIO_3 (A= Tl, α-Rb), *Chinese Journal of Physics* **59** (2019), 10 – 20, DOI: 10.1016/j.cjph.2019.02.019.

[10] E. L. Belokoneva, O. V. Reutova, O. V. Dimetrova and A. S. Volkov, Synthesis and crystal structure of a new iodate $(Pb_{0.6}Ba_{0.4})(Pb_{0.4}Ba_{0.6})[IO_3]_4$ analogous to $Sr[IO_3]_2$, *Crystallography Reports* **64** (2019), 590 – 593, DOI: 10.1134/S1063774519040047.

[11] J. G. Bergman, G. D. Boyd and A. Ashkin, New nonlinear optical materials: metal oxides with nonbonded electrons, *Journal of Applied Physics* **40** (1969), 2860 – 2863, DOI: 10.1063/1.1658089.

[12] P. Blaha, K. Schwarz, G. K. H. Madsen, D. Kvasnicka, J. Luitz, R. Laskowski, F. Tran and L. D. Marks, *WIEN2K An Augmented Plane Wave Plus Local Orbitals Program for Calculating Crystal Properties, User's Guide, WIEN2K_18.2*, Vienna University of Technology, Austria (2018).

[13] K. Chai and H. Li, Synthesis, characterization and theoretical calculation of a noncentrosymmetric compound, $Cs_{0.92}B_{0.92}Si_{5.08}O_{12}$, *Journal of Physics and Chemistry of Solids* **135** (2019), 109109, DOI: 10.1016/j.jpcs.2019.109109.

[14] M. Fuchs and M. Scheffler, Ab initio pseudopotentials for electronic structure calculations of polyatomic systems using density-functional theory, *Computer Physics Communications* **119** (1999), 67 – 98, DOI: 10.1016/S0010-4655(98)00201-X.

[15] P. Gong, F. Liang, L. Kang, X. Chen, J. Qin, Y. Wu and Z. Lin, Recent advances and future perspectives on infrared nonlinear optical metal halides, *Coordination Chemistry Review* **380** (2019), 83 – 102, DOI: 10.1016/j.ccr.2018.09.011.

[16] X. Gonze, J.-M. Beuken, R. Caracas, F. Detraux, M. Fuchs, G.-M. Rignanese, L. Sindic, M. Verstraete, G. Zerah, F. Jollet, M. Torrent, A. Roy, M. Mikami, Ph. Ghosez, J.-Y. Raty and D. C. Allan, First-principles computation of material properties: the ABINIT software project, *Computational Materials Science* **25** (2002), 478 – 492, DOI: 10.1016/S0927-0256(02)00325-7.

[17] Z. Hebboul, C. Galez, D. Benbertal, S. Beauquis, Y. Mugnier, A. Benmakhlouf, M. Bouchenafa and D. Errandonea, Synthesis, characterization, and crystal structure determination of a new lithium zinc iodate polymorph $LiZn(IO_3)_3$, *Crystals* **9** (2019), 464 – 475, DOI: 10.3390/cryst9090464.

[18] T. A. Hedge, A. Dutta, T. C. S. Girisun, M. Abith and G. Vinitha, Intensity tunable limiting behaviour of an organometallic cesium hydrogen tartrate single crystal, *Journal of Materials Science: Materials in Electronics* **30** (2019), 18885 – 18896, DOI: DOI: 10.1007/s10854-019-02245-5.

[19] R. Hill, The elastic behaviour of crystalline aggregate, *Proceedings of the Physical Society, Section A* 65 (1952), 349 – 354, DOI: 10.1088/0370-1298/65/5/307.

[20] Y. H. Kim, T. T. Tran, P. S. Halasyamani and K. M. Ok, Macroscopic polarity control with alkali metal cation size and coordination environment in a series of tin iodates, *Inorganic Chemistry Frontiers* **2** (2015), 361 – 368, DOI: 10.1039/C4QI00243A.

[21] W. Kohn and L. J. Sham, Self-consistent equations including exchange and correlation effects, *Physical Review Journals Archive* **140** (1965), A1133 – A1138, DOI: 10.1103/PhysRev.140.A1133.

[22] H. A. Kramers, The law dispersion and Bohr's theory of spectra, *Nature* **113** (1924), 673 – 674, DOI: 10.1038/113673a0.

[23] H. A. Kramers, The quantum theory of dispersion, *Nature* **114** (1924), 310 – 311, DOI: 10.1038/114310b0.

[24] R. de L. Kronig, On the theory of dispersion of X-rays, *Journal of the Optical Society of America* **12** (1926), 547 – 550, DOI: 10.1364/JOSA.12.000547.

[25] C. Li, P. Zhao, Z. Gao, Q. Wu, X. Tian, D. Ju, W. Lu, Y. Sun, D. Cui and X. Tao, Investigation into the optimized growth, anisotropic properties and theoretical calculations of the polar material $Cs_2TeW_3O_{12}$, *CrystEngComm* **21** (2019), 2345 – 2354, DOI: 10.1039/C9CE00111E.

[26] Y. Li, G. Han, H. Yu, H. Li, Z. Yang and S. Pan, Two polar molybdenum(VI) iodates(V) with large second-harmonic generation responses, *Chemistry of Materials* **31** (2019), 2992 – 3000, DOI: 10.1021/acs.chemmater.9b00521.

[27] J. Lin, Q. Liu, Z. Yue, K. Diefenbach, L. Cheng, Y. Lin and J-Q. Wang, Expansion of the structural diversity of f-element bearing molybdate iodates: synthesis, structures, and optical properties, *Dalton Transactions* **48** (2019), 4823 – 4829, DOI: 10.1039/C8DT05120H.

[28] C. H. M. Gillarvy and C. L. P. Van Eck, The crystal structure of sodium and ammonium iodate, *Recueil des Travaux Chimiques des Pays-Bas* **62**(11) (1943), 729 – 735, DOI: 10.1002/recl.19430621105.

[29] F.-F. Mao, C.-L. Hu, K. Chen and J.-G. Mao, A series of mixed-metal germanium iodates as second-order nonlinear optical materials, *Chemistry of Materials* **30** (2018), 2443 – 2452, DOI: 10.1021/acs.chemmater.8b00630.

[30] F. Mouhat and F.-X. Couder, Necessary and sufficient elastic stability conditions in various crystal systems, *Physical Review B* **90** (2014), 224104, DOI: 10.1103/PhysRevB.90.224104.

[31] R. E. Newnham, *Properties of Materials: Anisotropy, Symmetry, Structure*, Oxford University Press Inc., New York (2005).

[32] G. Peng, C. Lin, D. Zhao, L. Cao, H. Fan, K. Chen and N. Ye, $Sr[B(OH)_4](IO_3)$ and $Li_4Sr_5[B_{12}O_{22}(OH)_4](IO_3)_2$: two unprecedented metal borate-iodates showing subtle balance of enlarged gap and birefringence, *Chemical Communications* **48** (2019), 11139 – 11142, DOI: 10.1039/C9CC05021C.

[33] J. P. Perdew, S. Burke and M. Ernzerhof, Generalized gradient approximation mads sample, *Physical Review Letters* **77** (1996), 3865 – 3868, DOI: 10.1103/PhysRevLett.77.3865.

[34] J. P. Perdew and Y. Wang, Accurate and simple analytic representation of the electron-gas correlation energy, *Physical Review B* **45** (1992), 13244 – 13249, DOI: 10.1103/PhysRevB.45.13244.

[35] A. Pogu, P. W. Jaschin, K. B. R. Varma and K. Vidyasagar, Syntheses, structural variants and characterization of $A_2CdSn_2S_6$ (A = Cs, Rb and K) compounds, *Journal of Solid State Chemistry* **277** (2019), 713 – 720, DOI: 10.1016/j.jssc.2019.07.024.

[36] R. C. Powell, *Symmetry, Group Theory and the Physical Properties of Crystals*, Springer Science and Business Media, LLC (2010), DOI: 10.1007/978-1-4419-7598-0.

[37] S. F. Pugh, XCII. Relations between the elastic moduli and the plastic properties of polycrystalline pure metals, *The London, Edinburgh, and Dublin Philosophical Magazine and Journal of Science* **45** (1954), 823 – 843, DOI: 10.1080/14786440808520496.

[38] S. I. Ranganathan and M. Ostoja-Starzewski, Universal elastic anisotropy index, *Physical Review Letters* **101** (2008), 055504, DOI: 10.1103/PhysRevLett.101.055504.

[39] A. H. Reshak and S. Auluck, $LiMoO_3(IO_3)$, a novel molybdenyl iodate with strong second-order optical nonlinearity, *Journal of Alloys and Compounds* **660** (2016), 32 – 38, DOI: 10.1016/j.jallcom.2015.11.076.

[40] A. Reuss, Calculation of the flow limits of mixed crystals on the basis of the plasticity of monocrystals (Berechnung der Fließgrenze von Mischkristallen auf Grund der Plastizitätsbedingung für Einkristalle), *Zeitschrift für Angewandte Mathematik und Mechanik* **9** (1929), 49 – 58, DOI: 10.1002/zamm.19290090104.

[41] S. Saha and T. P. Sinha, Electronic structure, chemical bonding, and optical properties of paraelectric $BaTiO_3$, *Physical Review B* **62** (2000), 8828 – 8834, DOI: 10.1103/PhysRevB.62.8828.

[42] K. Schwarz, P. Blaha and G. K. H. Madsen, Electronic structure calculations of solid using the WIEN2K package for material sciences, *Computer Physics Communications* **147** (2002), 71 − 76, DOI: 10.1016/S0010-4655(02)00206-0.

[43] J. C. Slater, Wave functions in a periodic potential, *Physical Review Journals Archive* **51** (1937), 846 − 851, DOI: 10.1103/PhysRev.51.846.

[44] H. Song, N. Wang, Y. Li, Z. Lin, J. Yao and G. Zhang, SrI_3O_9H: a new alkaline earth metal iodate with two different anionic units using mild aqua-solution method, *Solid State Sciences* **97** (2019), 105982, DOI: 10.1016/j.solidstatesciences.2019.105982.

[45] R. E. Sykora, S. M. McDaniel, D. M. Wells and T. E. Albrecht-Schmitt, Mixed-metal uranium(VI) iodates: hydrothermal syntheses, structures, and reactivity of $Rb[UO_2(CrO_4)(IO_3)(H_2O)]$, $A_2[UO_2(CrO_4)(IO_3)_2](A = K, Rb, Cs)$, and $K_2[UO_2(MoO_4)(IO_3)_2]$, *Inorganic Chemistry* **41** (2002), 5126 − 5132, DOI: 10.1021/ic025773y.

[46] R. E. Sykora, K. M. Ok, P. S. Halasyamani and T. E. Albrecht-Schmitt, Structural modulation of molybdenyl iodate architectures by alkali metal cations in $AMoO_3(IO_3)$ (A = K, Rb, Cs): a facile route to new polar materials with large SHG responses, *Journal of the American Chemical Society* **124** (2002), 1951 − 1957, DOI: 10.1021/ja012190z.

[47] R. E. Sykora, K. M. Ok, P. S. Halasyamani, O. M. Wells and T. E. Albercht-Schmitt, New one-dimensional vanadyl iodates: hydrothermal preparation, structures, and NLO properties of $A[(VO_2)_2(IO_3)_3O_2](A = NH_4, Rb, Cs)$, *Chemistry of Materials* **14** (2002), 2741 − 2749, DOI: 10.1021/cm020021n.

[48] R. E. Sykora, D. M. Wells and T. E. Albrecht-Schmitt, Hydrothermal synthesis and structure of a new one-dimensional, mixed-metal U(VI) iodate, $Cs_2[(UO_2)(CrO_4)(IO_3)_2]$, *Inorganic Chemistry* **41** (2002), 2304 − 2306, DOI: 10.1021/ic020055x.

[49] C. Tang, X. Jiang, W. Yin, F. Chen, S. Guo, G. Song, L. Liu, H. Huang, M. Xia, Z. Lin and X. Wang, Rubidium cerium(IV) iodates with high UV-light-driven photocatalytic efficiency, *ChemistrySelect* **4** (2019), 7076 − 7081, DOI: 10.1002/slct.201901176.

[50] H.-X. Tang, Y.-X. Zhang, C. Zhuo, R.-B. Fu, H. Lin, Z.-J. Ma and X.-T. Wu, A niobium oxyiodate sulfate with a strong second-harmonic-generation response built by rational multi-component design, *Angewandte Chemie International Edition* **58**(12) (2018), 3824 − 3828, DOI: 10.1002/anie.201813122.

[51] R.-L. Tang, C.-L. Hu, B.-L. Wu, Z. Fang, Y. Chen and J.-G. Mao, $Cs_2Bi_2O(Ge_2O_7)$ (CBGO): a larger SHG effect induced by synergistic polarization of BiO_5 polyhedra and GeO_4 tetrahedra, *Angewandte Chemie International Edition* **58** (2019), 15358-15361, DOI: 10.1002/anie.201909735.

[52] R. F. Tinder, *Tensor Properties of Solids, Part One: Equilibrium Tensor Properties of Solids, Synthesis Lectures on Engineering*, Morgan & Claypool Publishers, 2007, 144 pages, DOI: 10.2200/S00057ED1V01Y200712ENG04.

[53] F. Tran and P. Blaha, Accurate band gaps of semiconductors and insulators with a semi-local exchange-correlation potential, *Physical Review Letters* **102** (2009), 226401, DOI: 10.1103/PhysRevLett.102.226401.

[54] N. Troullier and J. L. Martins, Efficient pseudopotentials for plane-wave calculations, *Physical Review B* 43 (1991), 1993 − 2006, DOI: 10.1103/PhysRevB.43.1993.

[55] W. Voigt, *Lehrbuch der Kristallphysik*, Terubner Verlag, Leipzig (1928).

[56] W. Chaoguo, The crystal structure of cesium iodate, *Acta Chimica Sinica* **43**(3) (1985), 271 − 274, http://sioc-journal.cn/Jwk_hxxb/EN/Y1985/V43/I3/271.

[57] L. Wheeler, S.I. Penfield, On some alkaline iodates (Über einige Alkali-jodate), Z. Anorg. Chem. 2(1) (1892), 437 – 447, DOI: 10.1002/zaac.18920020133.

[58] C. Wu, L. Lin, X. Jiang, Z. Lin, Z. Huang, M. G. Humphrey, P. S. Halasyamani and C. Zhang, $K_5(W_3O_9F_4)(IO_3)$: An efficient mid-infrared nonlinear optical compound with high laser damage threshold, *Chemistry of Materials* **31**(24) (2019), 10100 – 10108, DOI: 10.1021/acs.chemmater.9b03214.

[59] Q. Wu, X. Liu, S. Xu, H. Pi and Y. Li, Five new silver rare-earth iodates, $AgLn(IO_3)_4$ (Ln = Pr, Sm, Dy, Er and Tm): synthesis, structures and properties, *ChemistrySelect* **4** (2049), 8709 – 8712, DOI: 10.1002/slct.201900926.

[60] Z.-J. Wu, E.-J. Zhao, H.-P. Xiang, X.-F. Hao, X.-J. Liu and J. Meng, Crystal structures and elastic properties of superhard IrN_2 and IrN_3 from first principles, *Physical Review B* **76** (2007), 054115, DOI: 10.1103/PhysRevB.76.054115.

[61] W. H. Zachariasen, Skrifter utgitt av Det Norske Videnskap-Akademi i Oslo, I. Mat.-Naturw. Klasse **4** (1928), 6 – 166.

[62] M. Zhang, C. Hu, T. Abdudouwufu, Z. Yang and S. Pan, Functional materials design via structural regulation originated from ions introduction: a study case in cesium iodate system, *Chemistry of Materials* **30** (2018), 1136 – 1145, DOI: 10.1021/acs.chemmater.7b05252.

[63] Q. Zhang, H. Mushahali, H. Duan, M.-H. Lee and Q. Jing, The linear and nonlinear optical reponse of $CsGeX_3$ (X = Cl, Br, and I): the finite field and first principles investigation, *Optik* **179** (2019), 89 – 98, DOI: 10.1016/j.ijleo.2018.10.159.